Development of a simplified n-heptane/methane model for high-pressure direct-injection natural gas marine engines

Jingrui Li[a], Haifeng Liu[a]*, Xinlei Liu[b], Ying Ye[a], Hu Wang[a], Xinyan Wang[c], Hua Zhao[c], Mingfa Yao[a]

[a]State Key Laboratory of Engines, Tianjin University, Tianjin, 300072, P. R. China

[b]Clean Combustion Research Center, King Abdullah University of Science and Technology, Thuwal 23955-6900, Saudi Arabia

[c]Brunel University London, Kingston Lane, Uxbridge, Middlesex UB8 3PH, United Kingdom

*__Corresponding author:__ Haifeng Liu Tel.: 86-22-27406842ext8011; Fax: 86-22-27383362; Email: haifengliu@tju.edu.cn

Abstract

High-pressure direct-injection (HPDI) of natural gas is one of the most promising solutions for the future ship engines, for which the combustion process is mainly controlled by the chemical kinetics. However, the employment of detail chemical mechanisms for the multi-dimensional combustion simulation is significantly expensive due to the large scale of the marine engine. In the present study, a reduced n-heptane/methane mechanism consisted of 35-step reactions was constructed using multiple reduction approaches. Then this mechanism was further reduced to include only 27 reactions by the HyChem (Hybrid Chemistry) method. An overall good agreement with the experimentally measured ignition delay data of both n-heptane and methane for these two reduced mechanisms was achieved and reasonable predictions for the measured laminar flame speeds were obtained for the 35-step mechanism. But the 27-step mechanism cannot predict the laminar flame speed very well. In addition, these two reduced mechanisms were both able to reproduce the experimentally measured in-cylinder pressure and heat release rate profiles for a HPDI natural gas marine engine, although the engine-out CO emission was over-predicted and the NOx emission was slightly underestimated. The predicted distributions of temperature and equivalence ratio by the 35-step and 27-step mechanisms are similar with those of the 334-step mechanism. However, the predicted distributions of OH and CH_2O are significantly different from those of the 334-step mechanism. In short, the developed reduced chemical kinetic mechanisms provide a high-efficient and dependable method to simulate the characteristics of combustion and emissions in HPDI natural gas marine engines.

Keywords: High-Pressure Direct-Injection, Natural Gas, Chemical Kinetics, Combustion Modelling, Marine Engine

1. Introduction

In recent decades, the lower pollutant emissions and better fuel economy are the primary research targets to meet the more and more stringent emission regulations for internal combustion engines (ICEs) and deal with the potential oil shortage in the near future. Therefore, there is a worldwide interest in looking for clean alternative fuels for ICEs. Natural gas has attracted more and more attention due to its advantages of worldwide reserves and suitable combustion features in both the spark-ignited and compression ignition (CI) engines. Loads of research have revealed that high thermal efficiency and low pollutant emissions can be obtained for the natural gas engines. However, owing to its high-octane number and low reactivity, the natural gas is difficult to be ignited in CI engines compared to diesel fuel. As a result, when natural gas is taken as the fuel supply in CI engines, an additional ignition source like a spark plug or high-reactivity fuel should be implemented [1-6].

Different types of natural gas engines have been summarized in the literature [7]. There are primarily three kinds of operating modes for natural gas engines, which are pure natural gas engines, low-pressure dual-fuel engines, and high-pressure direct-injection dual-fuel engines. In pure natural gas engines, natural gas is ignited by a spark plug. Engine knock occurred at heave loads and misfire may occur at low load. Therefore, for pure natural gas engines, load expansion is an urgent problem [8]. In low-pressure dual-fuel engines, the engine operates with premixed natural gas and direct-injection pilot diesel, and the natural gas is typically introduced through the intake port during the intake stroke. Although knock and misfire are inhibited significantly by the pilot diesel, the power output and thermal efficiency are still limited by knock, and the low-load condition also meet with the instability problem [9]. In high-pressure direct-injection (HPDI) dual-fuel engines, both natural gas and pilot diesel are injected into cylinder near the top dead center. Pilot diesel is injected into cylinder prior to natural gas, when natural gas is injected into the cylinder, pilot diesel has been spontaneously ignited. The natural gas is entrained into the pilot flame and ignited. For HPDI dual-fuel engines, the performance can even match conventional diesel engines, while the emissions are lower. However, the original emissions of NOx and soot in the cylinder are still higher than

the limited values of regulations [10, 11].

Experiment methodology plays an important role in improving performance and emissions in natural gas engines. However, due to the complex combustion process in ICEs, the metal engine experiment is not able to explore the detailed combustion processes within the engine chamber, such as the ignition process, emission formation process, and combustion kinetics process [12, 13]. Therefore, the computational fluid dynamic (CFD) approach is usually adopted. There has been a continuous interest in the development of a better understanding of the detailed combustion process in ICEs, for which the CFD is frequently employed owing to its effectiveness and low expenses. In order to better predict the spray-combustion process occurring in engines, the chemical kinetic mechanism should be adopted in the CFD modeling study. However, the detailed combustion kinetic mechanism is typically consisted of hundreds of species and reactions, making it difficult to be directly coupled with the CFD codes. In addition, for the real fuels like diesel, it has hundreds of compositions, ranging from alkanes, alkenes, cyclic alkanes and alkenes, aromatics, and other stuff. Therefore, in order to better represent the chemical reactivity of diesel, researchers usually employ n-heptane as the surrogate fuel, due to its simple molecular structure and similar ignition/combustion feature with diesel [14, 15]. For natural gas, which is primarily composed of methane and minimal fractions of hydrogen, ethane, propane, or other mixtures depended on the sources and refinement methods, researchers usually adopt methane to predict the combustion process of natural gas. Many efforts have been devoted to studying the ignition process of n-heptane and methane in laboratory devices such as shock tubes [2, 16-22], flow reactors [23-25], rapid compression machines [26-29], and engines [30-32].

It is known that marine engines typically have much larger sizes compared to conventional automobile engines. As a result, the three-dimensional CFD modeling of the spray-combustion process for marine engines is significantly more expensive especially when coupled with the detailed chemical kinetics mechanism. Therefore, the development of reduced mechanisms with compact size but high reliability is urgently required. Lots of efforts have been made in the development of reduced n-heptane mechanisms. Seshadri et al. [33] developed a skeletal n-heptane mechanism with 23 species and 34

reactions and applied this mechanism to study the structure of premixed n-heptane flames. Peters et al. [34] developed a skeletal mechanism for n-heptane oxidation with 30 species based on a 56-step mechanism, which includes both the low- and high-temperature chemistries. Furthermore, this mechanism reproduced ignition delay times at various pressures and temperatures reasonably well. Tanaka et al. [28] developed a reduced mechanism for primary reference fuels and validated it with experimental data measured in a rapid compression engine (RCM) under a lean mixture condition. In this mechanism, the intermediate reactions involving species with carbon numbers from 2 to 5 were omitted and alkylketoperoxide were considered to undergo a single oxidation reaction to formCO. The mechanism was able to well predicted the ignition delay measured in the RCM but significantly underestimated the ignition delay measured in the shock tube. Li et al. [35] developed a reduced n-heptane mechanism composed of 20 species and 29 reactions. This mechanism not only describes the two oxidation stages of heptyl, the chain branch, as well as the chain propagation processes but also includes the peroxidation process of small alkyl radicals. Su and Huang [36] proposed a reduced n-heptane mechanism with 40 species and 62 reactions, which reproduced the two-stage ignition process of n-heptane and the performance of this mechanism generally agreed well with those of the detailed mechanism. Although the above mechanisms reproduced ignition delay times of n-heptane reasonably well, the methane sub-mechanism was not included or validated.

Patel et al. [37] et al. also constructed a reduced n-heptane mechanism consisted of 29 species and 52 reactions, in which the methane sub-mechanism was also included. This mechanism exhibited a similar predictive performance for the combustion of n-heptane with the detail mechanisms, while the ignition delays of methane were underestimated. Maroteaux and Noel [38] developed two reduced n-heptane mechanisms, including 61 and 26 reactions, respectively, and the methane sub-mechanisms were also included, which however, failed to well predict the ignition delays for methane. Lapointe et al. [39] developed an 8-step core sub-mechanism for n-heptane coupled with a C_0-C_4 sub-mechanism, which was consisted of hundreds of species and reactions, making it difficult to be adopted in the three-dimensional modeling study.

Based on the literature review, there has not been a reduced n-heptane/methane mechanism that is compact enough

(containing less than100 reactions) and is able to predict the experimentally measured ignition delays for both n-heptane and methane simultaneously well, which limits its application in an efficient and accurate simulation of large-size dual-fuel marine engines. Therefore, in the present study, firstly, a 35-step reduced chemical kinetic mechanism for n-heptane/methane was constructed by using various mechanism reduction approaches, including the reaction pathway analysis, sensitivity analysis, decoupling methodology, and chemical lumping methods. Then, based on the 35-step mechanism, a 27-step mechanism was also developed by using the HyChem (Hybrid Chemistry) approach, specially aimed at the high-temperature regime. Both of these two reduced mechanisms were validated against the experimentally measured ignition delays, species concentration profiles, and laminar flame speeds. Finally, these two reduced mechanisms were coupled with the CFD code to predict the engine combustion and emissions for a marine engine.

2. Model development

2.1 Development of the 35-step model

The reduced mechanism is primarily based on the detailed n-heptane mechanism developed by Curran et al. [14]. In this mechanism, the oxidation process of n-heptane is composed of two primary pathways, i.e. the low-temperature combustion (LTC) and high-temperature combustion (HTC) processes. Based on the reaction pathway analysis, CH_2O, HO_2, and H_2O_2 were identified as the most important intermediate species for the LTC reactions of n-heptane, which dominated its ignition process. During the LTC period, much H_2O_2 was generated, which was then decomposed just before the HTC period, leading to the rapid growth of OH and laying the foundation for the high-temperature ignition. Although the combustion of methane does not exhibit an obvious LTC feature, these species like CH_2O, HO_2, H_2O_2, and OH are also the most significant species for its ignition and heat release, which must be included in the reduced mechanism.

A schematic diagram of the model is shown in Figure 1. Fuel consumption is initiated by the abstraction of H from n-heptane by O_2 to form C_7H_{15} and HO_2 (R1). Due to the symmetric molecular structure of n-heptane, there are four heptyl isomer products. Based on the lumping reduction approach, only C_7H_{15} is employed in the reduced mechanism to represent

the four isomers. After the initial reaction stage, a small amount of H, HO_2, and OH are formed, which will dominate the further consumption of n-heptane by the H-abstraction reactions R2, R3, and R4. The sensitivity analysis demonstrates that R2 is less important for the ignition process of n-heptane in comparison to R3 and R4. Therefore, R2 is ignored in the reduced mechanism.

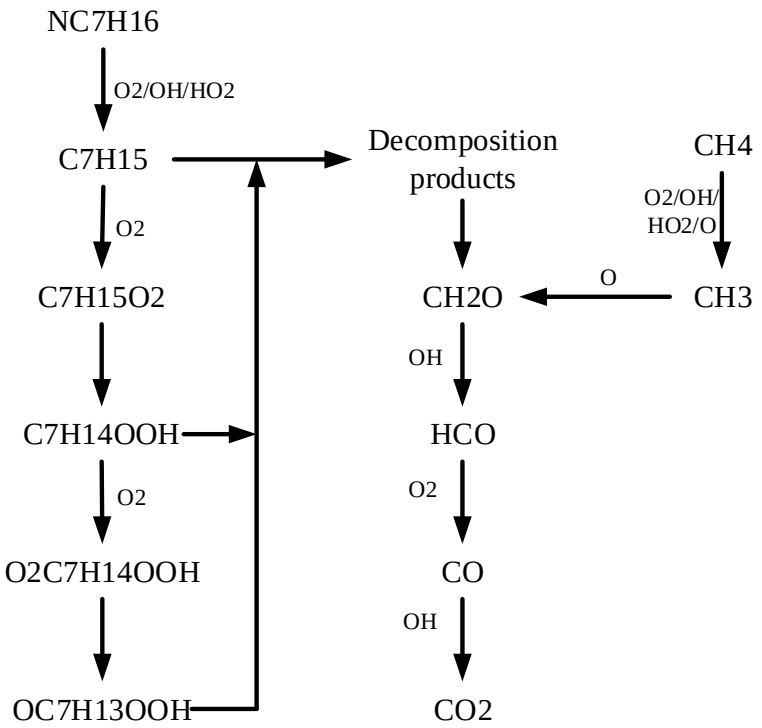

Fig. 1. *Reaction pathway of n-heptane/methane fuel blends oxidation.*

$$C_7H_{16} + O_2 \rightarrow C_7H_{15} + HO_2 \quad (R1)$$

$$C_7H_{16} + H \rightarrow C_7H_{15} + H_2 \quad (R2)$$

$$C_7H_{16} + HO_2 \rightarrow C_7H_{15} + H_2O_2 \quad (R3)$$

$$C_7H_{16}+OH \rightarrow C_7H_{15}+H_2O \quad (R4)$$

C_7H_{15} is then combined with O_2 to form $C_7H_{15}O_2$ (R5), which reaction is significantly sensitive to temperature. $C_7H_{15}O_2$ is primarily consumed via the isomerization process, generating $C_7H_{14}OOH$ (R6). After the second O_2-addition reaction (R7), $OOC_7H_{14}OOH$ is produced and then consumed by the decomposition reaction (R8), generating $OC_7H_{13}OOH$ and OH.

$$C_7H_{15} + O_2 \rightarrow C_7H_{15}O_2 \quad (R5)$$

$$C_7H_{15} \rightarrow C_7H_{14}OOH \quad (R6)$$

$$C_7H_{14}OOH + O_2 \rightarrow OOC_7H_{14}OOH \text{ (R7)}$$

$$OOC_7H_{14}OOH \rightarrow OC_7H_{13}OOH + OH \text{ (R8)}$$

At a higher temperature, $OC_7H_{13}OOH$ is further decomposed into $C_5H_{11}CO$, CH_2O, and OH in which $C_5H_{11}CO$ will also be consumed by the decomposition reactions, forming the smaller hydrocarbon products. To simplify this process, the decomposition reactions of $OC_7H_{13}OOH$ and $C_5H_{11}CO$ are lumped into one reaction (R9).

$$OC_7H_{13}OOH \rightarrow C_3H_7CO + CH_2O + OH \text{ (R9)}$$

At the high-temperature condition, the pyrolysis reactions become important. In the present study, only the β-decomposition reactions of C_7H_{15} and $C_7H_{14}OOH$ are considered, and the corresponding pyrolysis reactions are lumped into R10 and R11.

$$C_7H_{15} \rightarrow C_2H_4 + C_2H_5 + C_3H_6 \text{ (R10)}$$

$$C_7H_{14}OOH \rightarrow C_3H_6 + C_3H_7CHO + OH \text{ (R11)}$$

The skeletal C_2-C_4 sub-mechanism is taken from the works of Gustavsson et al. [40] and Zheng et al. [41] as the bridge between the n-heptane and methane sub-mechanisms, based on which a 16-step methane sub-mechanism was constructed as the base model. Finally, a reduced n-heptane/methane mechanism composed of 33 species and 35 reactions was developed and the reaction rate coefficients of some reactions were optimized based on the approach proposed by Ra and Reitz [42] to better predict the experimental results, the detailed n-heptane model and experimental data measured by Ciezki et al. [16] and Heufer et al. [43] were used to optimize the reaction rate coefficients. The final reduced model is shown in Table 1.

Table 1. The 35-step reduced mechanism and rate coefficients.

Number	Reaction	A	B	E	Ref
R1	NC7H16+O2=C7H15+HO2	7.00E+15	0	47380	[37], modified
	REV/	4.62E+11	0.3	172.0/	[37]
R2	OH+NC7H16=>C7H15+H2O	1.00E+14	0	3000	[35], modified
R3	C7H15+O2=C7H15O2	1.50E+12	0	0	[35], modified
	REV/	2.51E+13	0	27400.0/	[35]
R4	C7H15O2=C7H14OOH	8.94E+11	0	19000	[35], modified
	REV/	1.00E+11	0	11000.0/	[35]
R5	C7H14OOH+O2=OOC7H14OOH	2.20E+10	0	0	[35], modified

	REV/	2.51E+13	0	27400.0/	[35]
R6	OOC7H14OOH=>OC7H13OOH+OH	1.20E+11	0	17000	[35]
R7	OC7H13OOH=>C3H7CHO+CH2O+C2H3+OH	9.00E+14	0	41100	[37], modified
R8	C7H14OOH=>C3H6+C3H7CHO+OH	1.00E+13	0	25000	[35], modified
R9	C3H7CHO+OH=>C3H7CO+H2O	1.66E+12	0	0	[35]
R10	C3H7CO+O2=>CO+C3H6+HO2	6.03E+16	0	15000	[40]
R11	C7H15=>C2H4+C2H5+C3H6	7.04E+13	0	34600	[37], modified
R12	C3H7=>C2H4+CH3	9.60E+13	0	30950	[40]
R13	C2H5+O2=>C2H4+HO2	2.00E+10	0	-2200	[40]
R14	C2H4+OH=>C2H3+H2O	6.02E+13	0	5955	[40], modified
R15	C2H3+O2=>CH2O+HCO	4.00E+13	0	-251	[40]
R16	C3H6+OH=>C3H5+H2O	3.12E+06	2	-298	[40]
R17	C3H5+O2=>CH3+CH2O+CO	4.00E+12	0	0	[40]
R18	CH3+HO2=>CH3O+OH	5.00E+13	0	0	[40]
R19	CH3+O=>CH2O+H	8.00E+13	0	0	[40]
R20	CH4+O2=CH3+HO2	2.02E+07	2.1	53210	[42], modified
R21	CH4+OH=CH3+H2O	1.83E+05	2.6	2190	[42], modified
R22	CH4+O=CH3+OH	1.02E+09	1.5	8604	[42], modified
R23	CH4+HO2=CH3+H2O2	1.13E+01	3.7	21010	[42], modified
R24	CH3O+O2=>CH2O+HO2	2.41E+14	0	5017	[41]
R25	CH2O+OH=>HCO+H2O	3.47E+09	1.2	-477	[41]
R26	HCO+O2=>CO+HO2	1.35E+13	0	400	[40]
R27	CO+O+M=>CO2+M	4.17E+14	0	3000	[41]
R28	CO+OH=CO2+H	3.51E+07	1.2	69	[41]
	REV/	9.45E+13	0	26089.0/	[41]
R29	H2O2+M=>2OH+M	1.20E+17	0	45500	[41]
R30	HO2+HO2=>H2O2+O2	2.00E+12	0	0	[41]
R31	H+O2=O+OH	2.63E+16	-0.7	17040	[41]
	REV/	7.87E+13	-0.3	-278.0/	[41]
R32	H+O2+M=HO2+M	2.80E+18	-0.9	0	[41]
	REV/	4.66E+18	-0.9	48023.0/	[41]
R33	H2+OH=H2O+H	1.17E+09	1.3	3626	[40]
	REV/	1.24E+10	1.2	19092.0/	[40]
R34	O+H2=OH+H	5.06E+04	2.7	6290	[40]
	REV/	2.37E+04	2.7	4287.0/	[40]
R35	HO2+OH=>H2O+O2	7.50E+12	0	0	[40]

2.2 Development of the 27-step model

In the HPDI natural gas engines, which typically have the higher compression ratio, the temperature at the top dead center is high (around 1000 K) than the conventional engines. As discussed in Section 2.1, during the HTC process, the LTC reaction pathway is less significant and n-heptane is primarily consumed by the decomposition reactions, converting into

small hydrocarbons. Therefore, the 35-step mechanism was further reduced for the HTC regime by using the HyChem approach. which employs a physics-based understanding of the primary reaction pathways in fuel combustion, the more detailed introduction can be found in Ref. [44]. During the reduction, the O_2-addition reactions and the following LTC reaction pathway were removed, forming a new reduced n-heptane/methane mechanism consisted of 23 species and 27 reactions. Since the LTC reactions for n-heptane were removed, the reaction rate parameters were further optimized based on the sensitivity analysis. Noted that there was no change in the methane sub-mechanism. The final reduced model is shown in Table 2.

Table 2. The 27-step reduced mechanism and rate coefficients.

Number	Reaction	A	B	E	Ref
R1	NC7H16+O2=C7H15+HO2	1.00E+16	0	47380	[37], modified
	REV/	4.62E+11	0.3	172.0/	[37]
R2	OH+NC7H16=>C7H15+H2O	5.00E+13	0	3000	[35], modified
R3	HO2+NC7H16=C7H15+H2O2	9.01E+13	0	16000	[35], modified
	REV/	6.31E+10	0	8000.0/	[35]
R4	C7H15=>C2H4+C2H5+C3H6	7.04E+13	0	34600	[37], modified
R5	C2H5+O2=>C2H4+HO2	2.00E+10	-0.9	-2200	[40], modified
R6	C2H4+OH=>C2H3+H2O	6.02E+14	0	5955	[40], modified
R7	C2H3+O2=>CH2O+HCO	4.00E+13	0	-251	[40]
R8	C3H6+OH=>C3H5+H2O	3.12E+06	2	-298	[40]
R9	C3H5+O2=>CH3+CH2O+CO	4.00E+12	0	0	[40]
R10	CH3+HO2=>CH3O+OH	5.00E+13	0	0	[40]
R11	CH3+O=>CH2O+H	8.00E+13	0	0	[40]
R12	CH4+O2=CH3+HO2	2.02E+07	2.1	53210	[42], modified
R13	CH4+OH=CH3+H2O	1.83E+05	2.6	2190	[42], modified
R14	CH4+O=CH3+OH	1.02E+09	1.5	8604	[42], modified
R15	CH4+HO2=CH3+H2O2	1.13E+01	3.7	21010	[42], modified
R16	CH3O+O2=>CH2O+HO2	2.41E+14	0	5017	[41]
R17	CH2O+OH=>HCO+H2O	3.47E+09	1.2	-477	[41]
R18	HCO+O2=>CO+HO2	1.35E+13	0	400	[40]
R19	CO+O+M=>CO2+M	4.17E+14	0	3000	[41]
R20	CO+OH=CO2+H	3.51E+07	1.2	69	[41]
	REV/	9.45E+13	0	26089.0/	[41]
R21	H2O2+M=>2OH+M	1.20E+17	0	45500	[41]
R22	HO2+HO2=>H2O2+O2	2.00E+12	0	0	[41]
R23	H+O2=O+OH	2.63E+16	-0.7	17040	[41]
	REV/	7.87E+13	-0.3	-278.0/	[41]
R24	H+O2+M=HO2+M	2.80E+18	-0.9	0	[41]

	REV/	4.66E+18	-0.9	48023.0/	[41]
R25	H2+OH=H2O+H	1.17E+09	1.3	3626	[40]
	REV/	1.24E+10	1.2	19092.0/	[40]
R26	O+H2=OH+H	5.06E+04	2.7	6290	[40]
	REV/	2.37E+04	2.7	4287.0/	[40]
R27	HO2+OH=>H2O+O2	7.50E+12	0	0	[40]

2.3 Validations of the 35-step and 27-step models

Validation of the reduced mechanism was performed by comparing with the experimental data and the prediction of a 79 species and 334-step reactions n-heptane/methane mechanism [7]. The modeling target was a zero-dimensional combustion reactor under the constant-volume and adiabatic condition based on the SENKIN code. Figure 2 compares the experimental and calculated ignition delays for n-heptane under a wide range of ambient pressures from 13 atm to 55 atm and ambient temperatures from 700 K to 1200 K [19, 43, 45]. It is seen that the 35-step mechanism demonstratesa better agreement with experimental data than that of the 334-step mechanism under 13 atm and 38 atm, especially under the low and intermediate temperature region. The 27−step mechanism can well reproduce the ignition delay times for n-heptane under high temperatures and all the research pressures. Figure 3 compares the calculated and measured ignition delays for methane [20] under an ambient pressure of 10 atm and an initial temperature from 1300 K to 1700 K. The result demonstrates that there is no obvious negative temperature combustion region for the methane combustion. The predicted ignition delay times of methane for the 35-step and 27-step mechanisms show better agreement with the experimental data compared to the 334-step mechanism under high equivalence ratio conditions, whereas the 334-step mechanism performs better under low equivalence ratio conditions. In general, both of the two reduced mechanisms (35- and 27-step models) exhibited the good agreement with experimental data.

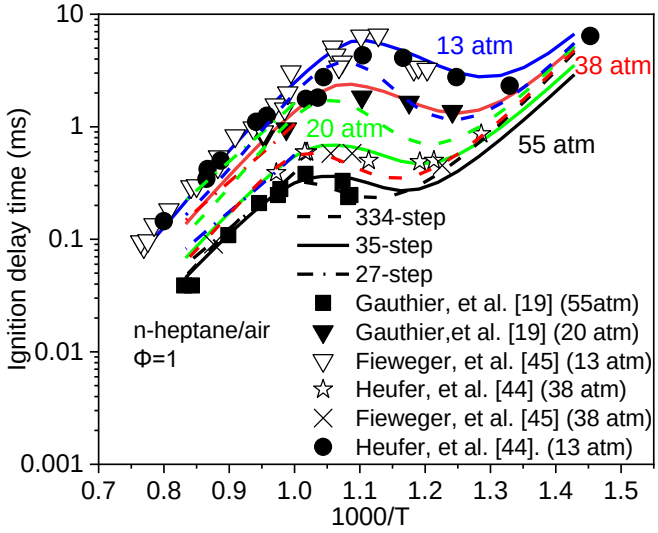

Fig. 2. Comparison of the predicted and measured ignition delay time for n-heptane/air mixture at Φ=1 (the black line represents 55 atm, the red line represents 38 atm, and the blue line represents 13 atm).

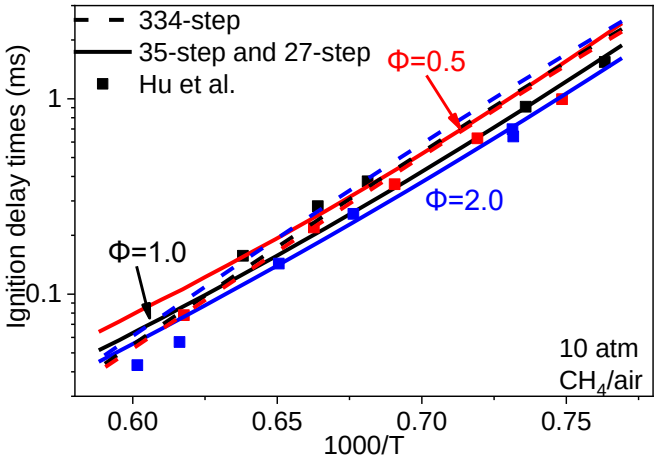

Fig. 3. Comparison of the predicted and measured ignition delay time for methane/air mixture under Φ=1 (The square symbol is experimental data).

Figures 4 and 5 compare the predicted species concentration profiles for the main species by the three reduced kinetic mechanisms in a constant volume chamber. Compared to the 334-step mechanism, the generally lower n-heptane consumption rate and peak C_2H_4 concentration were predicted by the 35-step mechanism. The consumption rate of methane for the 35-step mechanism is also slightly slower than that of the 334-step mechanism. However, the CH_2O profile of the 35-step mechanism is much higher than that of the 334-step mechanism. It is because that a part of CH_3 for the 334-step mechanism is oxidized to form CH_2 species, while for the 35-step mechanism, CH_2O is the only oxidation species.

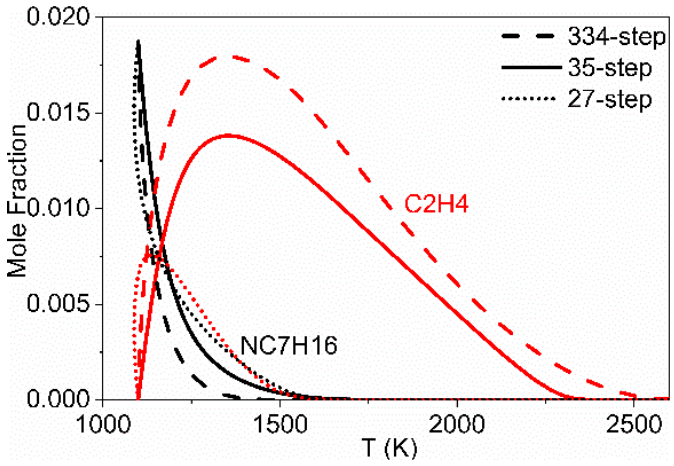

Fig. 4. Comparison of the predicted species concentration profiles for the n-heptane/air mixture under Φ=1.0, initial temperature of 1100 K, and pressure of 28 bar.

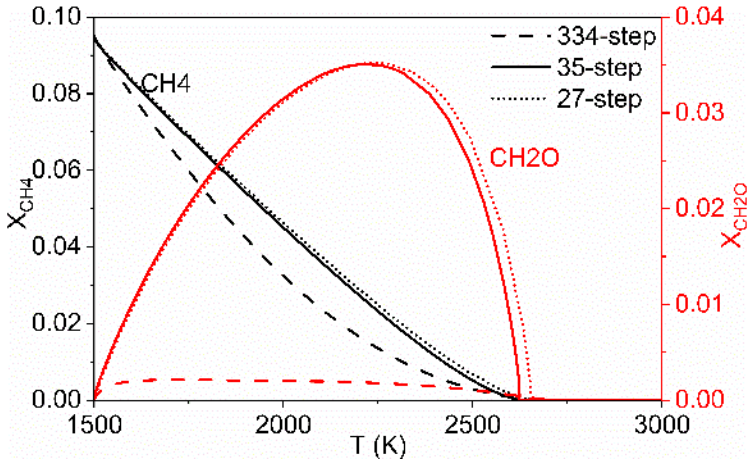

Fig. 5. Comparison of the predicted species concentration profiles for methane/air mixture under Φ=1.0, initial temperature of 1500 K, and pressure of 10 bar.

Comparisons between the calculated and experimental laminar flame speeds [46-57] of the n-heptane/air and methane/air mixtures at 1 bar are shown in Figs. 6 and 7, respectively. The predicted laminar flame speeds for the n-heptane/air mixture of the 334-step mechanism are in good agreement with the experimental data measured by Kumar et al. [46] and Dirrenberg et al. [50]. For the 35-step mechanism, it can reasonably reproduce the experimental data at the equivalence ratio of less than 1.3 for the n-heptane/air mixture. However, it significantly over-predicted the flame speed at the equivalence ratio of more than 1.3. The 27-step mechanism cannot reproduce laminar flame speeds of the n-heptane/air

mixture at all research equivalence ratio. For the methane/air flame as shown in Fig. 7, it is seen that the predicted laminar flame speed by the 334-step mechanism agrees well with the experimental values, except those measured by Bradley et al. [52], which is higher at the lean-fuel side and lower at the rich-fuel side. Whereas the predicted laminar flame speed by the 35-step and 27-step mechanisms are in good agreement with experimental data obtained by Bradley et al. [51] at the equivalence ratio less than 1.0, but they both significantly over-predict the experimental values at rich conditions.

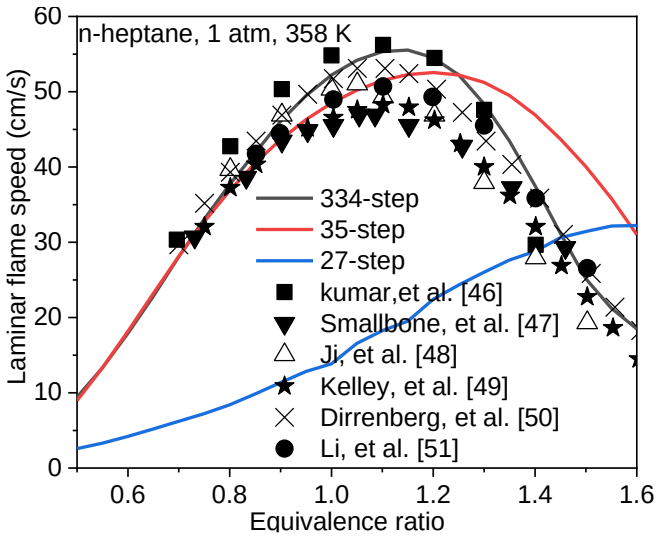

Fig. 6. Comparison of the predicted and measured laminar flame speeds for n-heptane/air mixtures under an initial temperature of 358 K and pressure of 1 bar (The square symbol is experimental data).

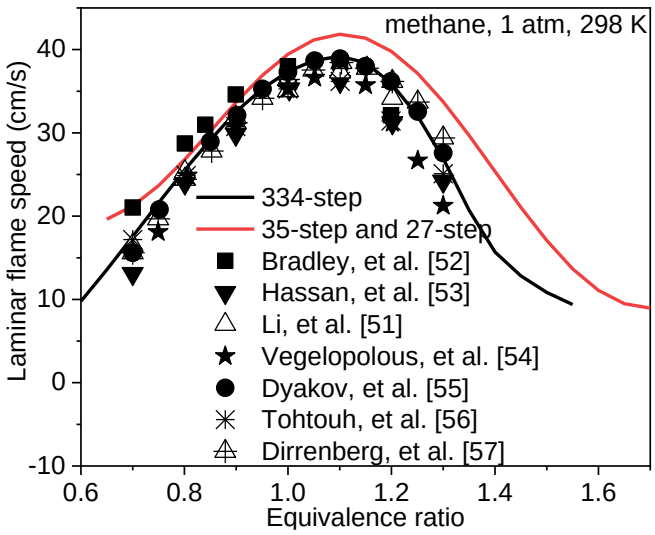

Fig. 7. Comparison of the predicted and measured laminar flame speeds of the methane/air mixture under an initial temperature of 298 K and pressure of 1 bar.

3. Mechanism validation in a marine engine

The final purpose of the reduced mechanisms is to be employed for the multi-dimensional CFD modeling studies. For the dual-fuel HPDI natural gas engine, it usually operates at around the stoichiometric- and lean burn conditions. As a result, it is preferably the reduced n-heptane/methane is able predict the ignition delay of n-heptane and laminar flame speed of methane well under such conditions. Based on the previous validations, it is seen that these two newly developed reduced mechanisms can reasonably predict the experimental results under the stoichiometric- and lean-burn conditions. In this section, they are further adopted for the 3D CFD modeling validations.

The engine combustion experiment was conducted on a Man Diesel & Turbo 4T50ME-GI engine, which was a low-speed and two-stroke marine engine. The main specifications of the engine can be found in Table 3 and the detailed parameters can be found in Ref. [7]. The computational study was performed using the Converge code [58]. A whole mesh with the highest cell number of about 1.5 million was adopted. The SAGE solver was adopted to simulate the detailed combustion chemistry. The extended Zeldovich model [59] and Hiroyasu soot model [60] were used to simulate the NOx and soot emissions, respectively. Detailed descriptions of the related sub-models used in the simulation can be found in Ref. [61]. It should be noted that all the boundary conditions in simulations were the same for the three reduced mechanisms. Table 4 lists the CPU-hour using the three mechanisms. Comparatively, it demonstrates that both the 27- and 35-step mechanisms can significantly reduce the computational expenses. Note that the current engine is in a large size, which needs more grids for simulations. With a higher grid number, the computational expenses will be further increased.

Table 3. *Main specifications of the 4T50ME-GI research engine.*

Parameters	Value
Type	4T50ME-GI
Number of cylinders	4
Bore/stroke	500 mm/2200 mm
Connecting rod	2885 mm
Geometric compression ratio	18.14
Engine speed @ MCR	123 rpm
Power @ MCR	7050 kW
IMEP @ MCR	20 bar
Turbocharger	MAN TCA55-VTA

Table 4. The CPU-hour of the three CFD models.

	334-step	35-step	27-step
CPU-hour	96	49	47

Figure 8 shows the measured and calculated pressure and heat release rate (HRR) profiles. The calculated pressure profiles of the three reduced mechanisms are all in good agreement with the experimental data. Comparatively, the calculated HRR profiles of the 27- and 35-step mechanisms are slightly higher than that of the experimental data and the 334-step mechanism, indicating that the combustion rates of both the 27- and 35-step mechanisms are also slightly higher. The previous study demonstrated that the combustion process for the HPDI natural gas engine was categorized into five stages, including the ignition delay period of the pilot-fuel, premixed combustion period of the pilot-fuel, rapid combustion period of methane, mixing-controlled combustion period, and the post-combustion period [62]. It is noticed that the premixed combustion stage for the pilot fuel of the 27-step mechanism is more intense than the other two mechanisms, owing to its predicted lower reactivity of n-heptane and thus the longer fuel-air mixing process. However, the pilot-fuel ignition timing of the 27-step mechanism is closer to the experimental data. Therefore, the maximum pressure (P_{max}) for the 27-step mechanism is in better agreement with experimental data.

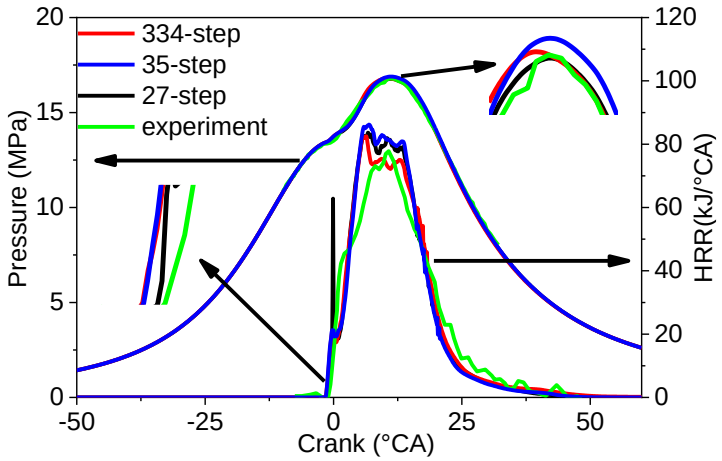

Fig. 8. Comparison of the predicted and measured for in-cylinder pressure and HRR profiles.

Comparisons of the predicted and measured primary parameters on combustion and engine performance are presented

in Table 4. For the key combustion parameters, the calculated CA10 and CA50 (CA10 and CA50 are defined as the crank angles that releases 10% and 50% of the heat.) for the three mechanisms are all in good agreement with the experimental data, and the highest error is less than 6.5% for both the 35- and 27-step mechanism compared with the experimental data. In addition, both the 35- and 27-step mechanisms are able to reproduce the maximum combustion pressure (P_{max}) and the corresponding phase ($P_{max\ phase}$), and the 27-step mechanism showing a better prediction performance. For the key engine performance parameters, the calculated power outputs and indicated specific fuel consumption (ISFC) of the 27- and 35-step mechanisms are in good agreement with the experimental data and the errors are less than 0.5%. This indicates that the 35- and 27-step mechanisms can be applied for the development of marine engines and prediction of important performance (such as power, fuel consumption) with high credibility, despite some deviations in its chemical kinetics (intermediate species, laminar flame speed) verification. Meanwhile, the important macroscopic combustion parameters of the engine captured by the 35-step mechanism are also relatively accurate, which can be applied to the development of the combustion system for engines.

Table 5. Comparison between the calculated and measured combustion parameters.

	27-step (error)	35-step (error)	334-step (error)	Experiment
CA10 (°CA ATDC)	3.7 (1.08%)	3.8 (3.68%)	4.0 (8.5%)	3.66
CA50 (°CA ATDC)	10.8 (5.56%)	10.7 (6.54%)	11.1 (2.7%)	11.4
P_{max} (MPa)	16.76 (0.36%)	16.89 (0.42%)	16.73 (0.53%)	16.82
$P_{max\ phase}$ (°CA ATDC)	11.2 (2.1%)	11.2 (2.1%)	10.9 (4.72%)	11.44
ISFC (g/kW·h)	164.0 (0.49%)	163.5 (0.18%)	164.6 (0.86%)	163.2
Power output (kW)	5331.8 (0.01%)	5346.7 (0.29%)	5311.6 (0.36%)	5331

Table 6 presents the experimental and predicted engine-out emissions. Overall, the predicted NOx emissions for the three reduced mechanisms are in good agreement with the experimental data, with the highest predicted errors less than 12.9%. At present, NOx is the only pollutant emission limited in IMO Tier III, thus the present 35- and 27-step mechanisms can be employed for the NOx emission prediction.

Table 6. Comparison between the calculated and measured emissions.

	27-step (error)	35-step (error)	334-step (error)	Experiment
NOx (g/kW·h)	10.68 (11.4%)	10.54 (12.9%)	11.37 (4.93%)	11.9

HC (g/kW·h)	0.0045	0.0039	0.0057	--
CO (g/kW·h)	0.0237 (700%)	0.0092 (1900%)	0.0351 (441%)	0.19
CO_2 (g/kW·h)	415.7	415.0	416.9	--
Soot (g/kW·h)	0.243	0.241	0.0238	--

In addition, similar predictions of the HC and CO_2 emissions are also observed for three reduced mechanisms. However, the calculated CO emissions are all significantly lower than the experimental values, owing to the predicted higher combustion rates, as shown in Fig. 5. And the predicted soot emissions of the 27- and 35-step mechanisms are an order of magnitude higher than that of the 334-step mechanism. Due to the complex combustion processes of engines, it is always difficult to accurately predict the incomplete combustion products, such as HC, CO, and soot. Further improvement work needs to be perform in the future.

Table 7 depicts the predicted in-cylinder temperature distributions for different mechanisms. The initial temperature distribution (0°CA) for the three mechanisms is almost the same. At 5°CA ATDC, the temperature distribution regions of the three mechanisms are similar, however, the local regions of the 35- and 27-step mechanisms have a higher temperature than that of the 334-step mechanism. This indicates that the combustion process of the 35- and 27-step mechanisms are more intense. At 10°CA ATDC, the temperature distributions of the three mechanisms are also similar, however, the local high-temperature regions of the 35- and 27-step mechanisms become larger than the 334-step mechanism, the intense combustion process leads to a higher heat release rate (seen in Figure 8).

35- and 27-step*Table 7. The predicted in-cylinder temperature distributions calculated by different reduced mechanisms.*

	0° CA	5° CA	10° CA	15° CA	20° CA
334-step	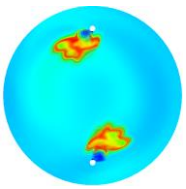	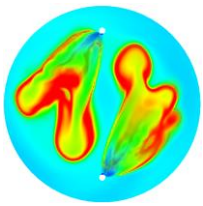	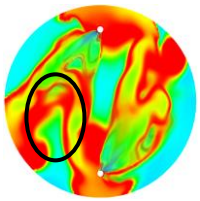	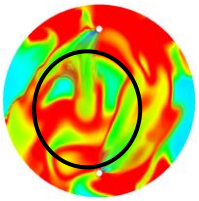	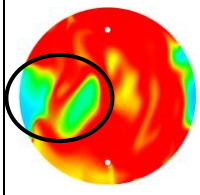

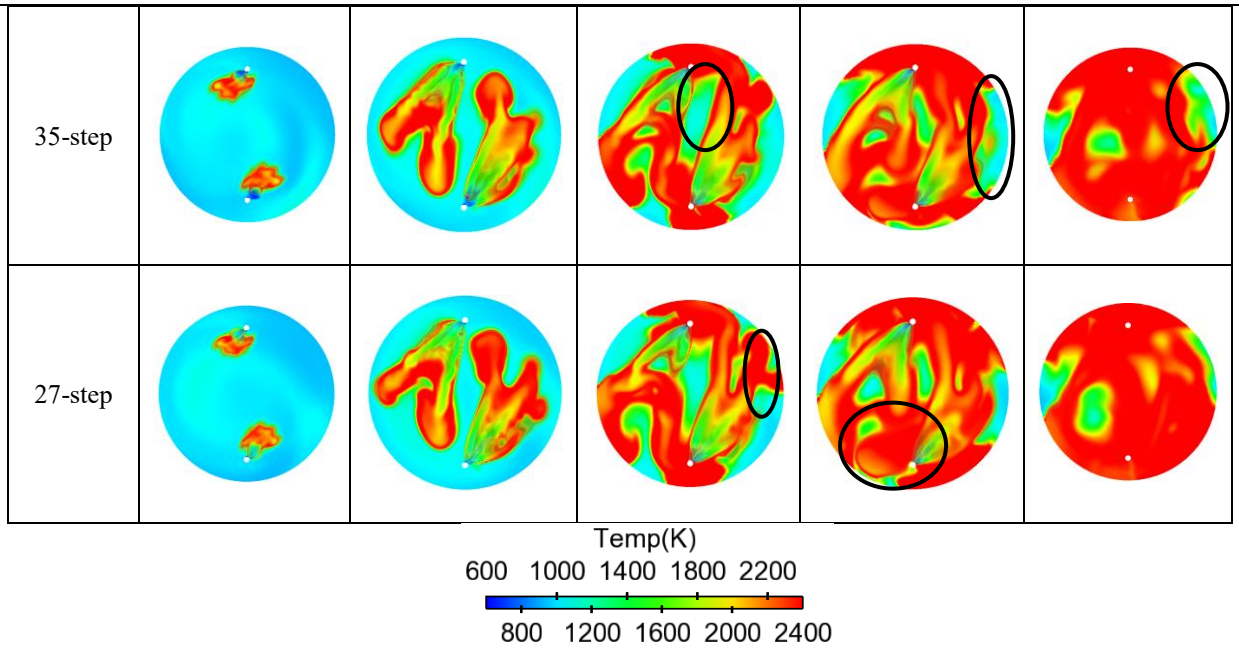

Table 8 shows the predicted equivalence ratio distributions of the three mechanisms. The equivalence ratio distributions of the three mechanisms are almost the same at 0°, 5°, and 10°CA ATDC. At 15°CA ATDC, however, the equivalence ratio distributions of the three mechanisms become different owing to the more significant effect of in-cylinder turbulent flows. Due to the more intense combustion process of the 35- and 27-step mechanisms, the fuel distributions of the 35- and 27-step mechanisms are wider. Correspondingly, the high-temperature regions are larger than the 334-step mechanism. Moreover, the combustion process of the 27-step mechanism is more intense than the 35-step mechanism, hence the high-temperature regions of the 27-step mechanism are slightly larger than the 35-step mechanism. At 20°CA ATDC, the high-temperature regions of the 27-step mechanism are larger than those of the 35-step and the 334-step mechanisms, and the fuel distribution regions are wider than those of the 35- and 334-step mechanisms. The main differences in temperature and equivalence ratio distributions for the three mechanisms are marked by the black circles.

Table 8. The predicted in-cylinder equivalence ratio distributions calculated by different reduced mechanisms. (The black line with the arrow represents the airflow motion, from which the contribution of the entrainment of the high-speed gas jet on the in-cylinder mixing)

	0° CA	5° CA	10° CA	15° CA	20° CA

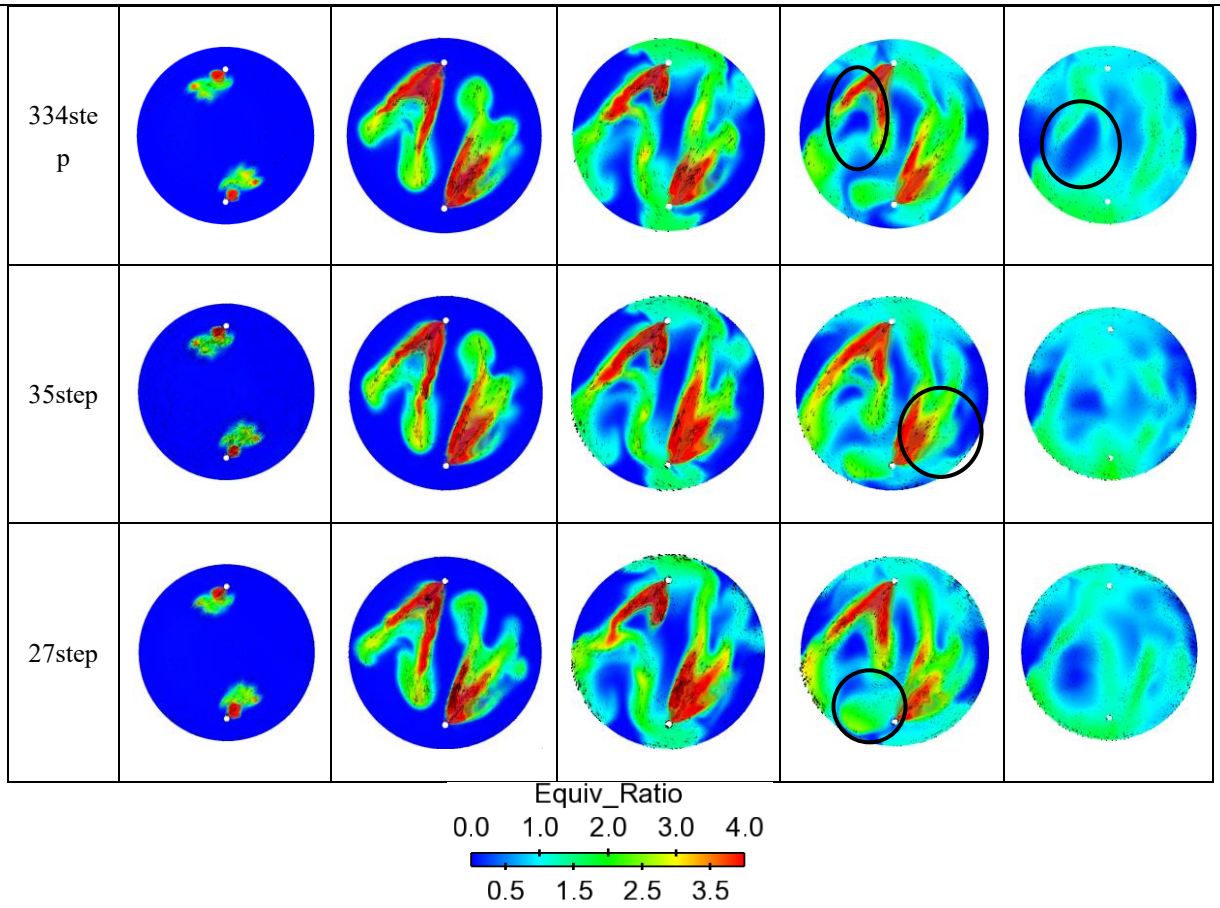

Table 9 shows the OH distributions of the three mechanisms. From 0° to 10° CA ATDC, the OH distributions of the three mechanisms are almost the same. It is well known that OH is the most important radicals at high-temperature combustion stage, thus the OH distribution is used to indicate high-temperature combustion region in the present study. As can be seen in Table 8 that the burning region can be clearly distinguished from the unburning region. According to a previous study [63], the initial combustion stage of the HPDI engine belongs to the premixed combustion, which can be demonstrated by the OH distributions at 0° and 5° CA ATDC. At 10°, 15°, and 20° CA ATDC, the OH distributions of the three mechanisms become different. It is interesting that high OH concentration regions of the 334-step mechanism are larger than the 35- and 27-step mechanism. It is because that the OH is concentrated on the edge of the high-temperature regions, while the high-temperature regions of the 35- and 27-step mechanisms are distributed almost throughout the cylinder, thus the high OH concentration regions are smaller. The main differences of OH distribution for the three mechanisms are marked in the black circles.

Table 9. The in-cylinder OH distributions calculated by different reduced mechanisms.

	0° CA	5° CA	10° CA	15° CA	20° CA
334step	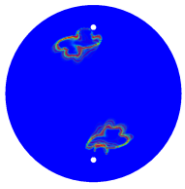	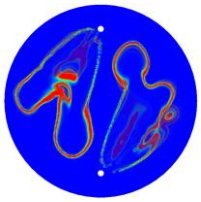	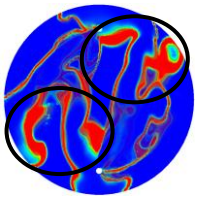	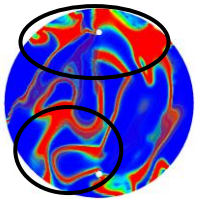	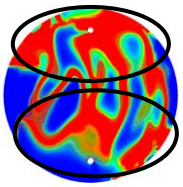
35step	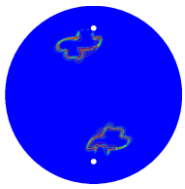	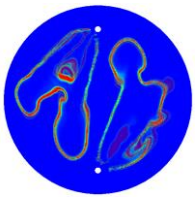	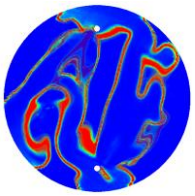	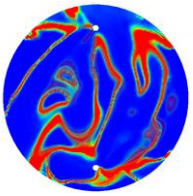	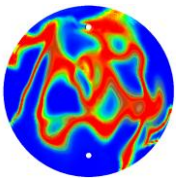
27step	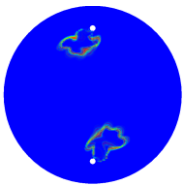	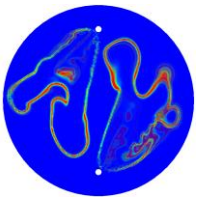	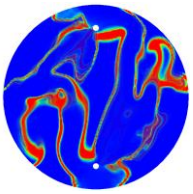	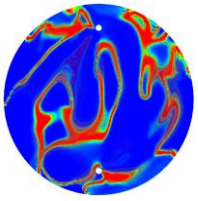	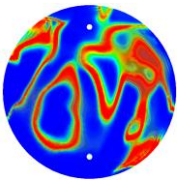

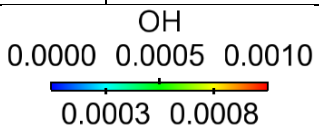

The CH_2O distributions of the three mechanisms are shown in Table 10. CH_2O is an important species at low combustion stage for n-heptane, and it is also an important species for the oxidation process of methane. At 0° CA ATDC, the CH_2O distributions of the 35- and 27-step mechanisms are much larger than that of the 334-step mechanism. For the 334-step mechanism, only a small amount of CH_2O concentrates near the nozzle. At 5° CA ATDC, the OH distribution of the 334-step mechanism becomes slightly larger, but it is also much smaller than those of the 35- and 27-step mechanisms, and the CH_2O concentration is also much lower than those of the 35- and 27-step mechanism. At 10° CA ATDC, the combustion process becomes intense, the formed CH_2O is instantly oxidized to HCO, therefore, the CH_2O of the 334-step mechanism disappears, and only a small amount of CH_2O concentrates near the nozzle for the 35- and 27-step mechanisms. At 15° CA and 20° CA ATDC, the CH_2O disappears in the cylinder for the 334- and 35-step mechanisms. However, the CH_2O concentration of the 27-step mechanism increases at 15° CA ATDC. The main differences of CH_2O distribution for the three

mechanisms are marked by the black circles.

Table 10. The in-cylinder CH_2O distributions calculated by different reduced mechanisms.

	0° CA	5° CA	10° CA	15° CA	20° CA
334-step	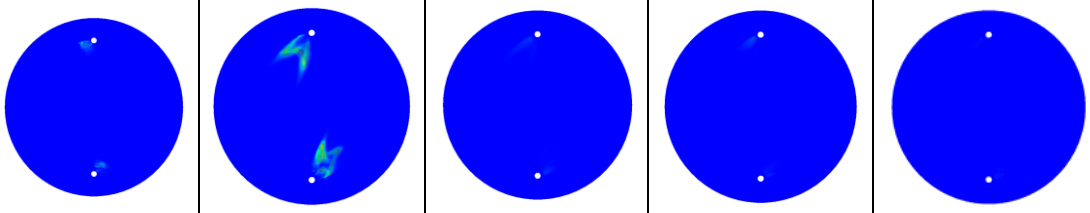				
35-step	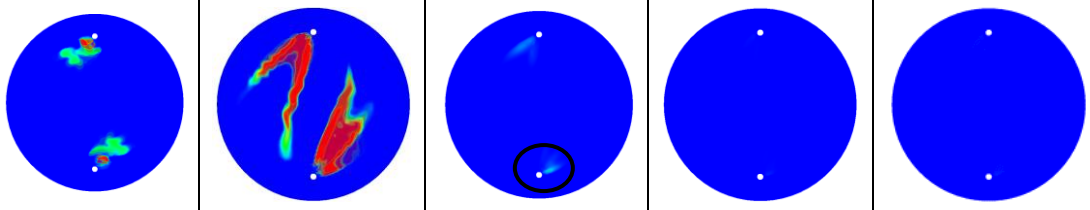				
27-step	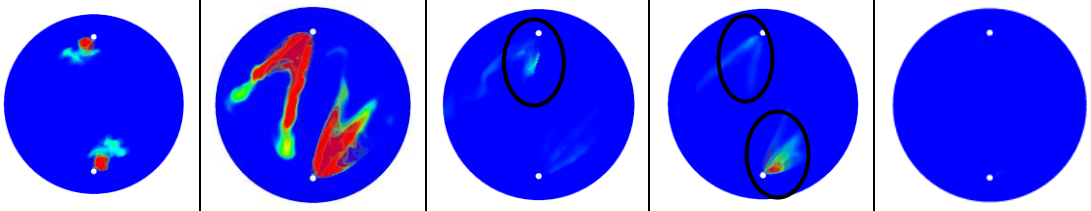				

Tables 11 and 12 depicts the predicted distribution of NOx and soot in the combustion process. Due to the later ignition timing of the 27-step mechanism, the NOx formation is lower at 0° CA ATDC. At 10° CA, the NOx distribution regions of the three mechanisms are similar. Due to differences in high-temperature distribution region, the NOx distribution regions of the three mechanisms are significantly different at 20° CA and 30° CA ATDC. However, the area of NOx distribution for the three mechanisms is similar. In general, the soot distribution regions of the three mechanisms are similar at different crank angles. However, the predicted soot concentration of the 334-step mechanisms is much lower than the 35- and 27-step mechanisms. The main differences in NOx and soot distributions for the three mechanisms are marked by the black circles.

Table 11. The in-cylinder NOx distributions calculated by different reduced mechanisms.

	0° CA	10° CA	20° CA	30° CA
334step	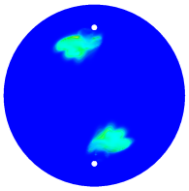	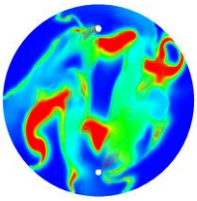	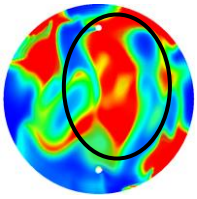	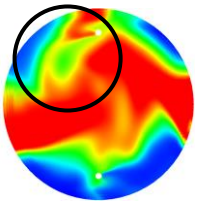
35step	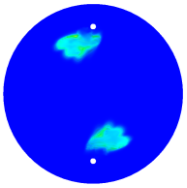	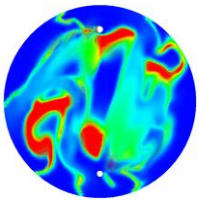	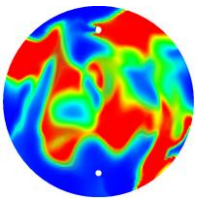	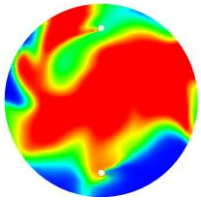
27step	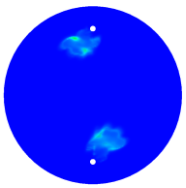	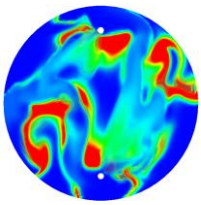	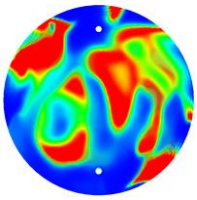	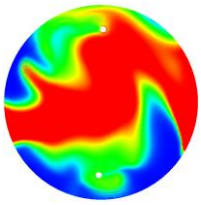

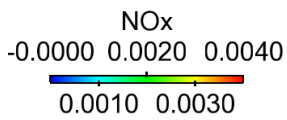

Table 12. The in-cylinder soot distributions calculated by different reduced mechanisms.

	0° CA	10° CA	20° CA	30° CA
334step	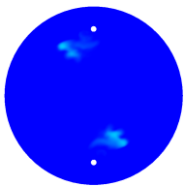	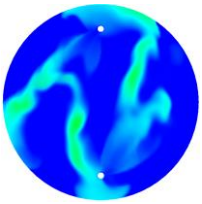	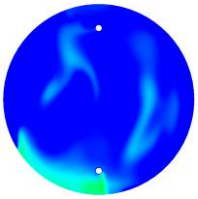	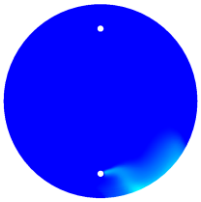
35step	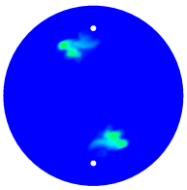	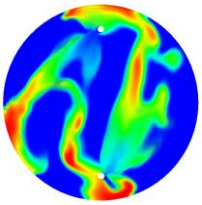	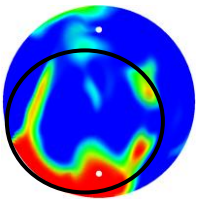	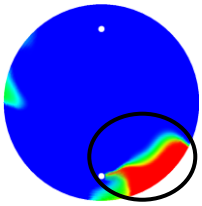

27step	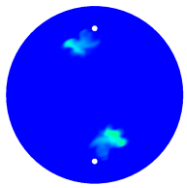	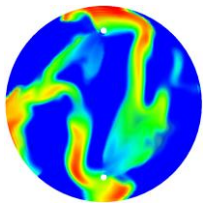	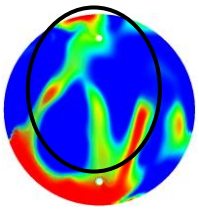	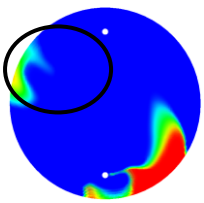	

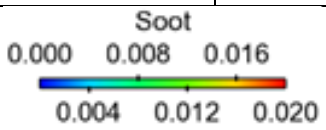

In summary, the 35-step mechanism can reproduce the ignition delay times of n-heptane at all research temperatures, while the 27-step mechanism gives reasonable predictions of ignition delay times for n-heptane at high temperatures. Both of these two mechanisms give well predictions of ignition delay times for methane. The main species histories of n-heptane and methane cannot be well reproduced by both the 27- and 35-step mechanism. In addition, the calculated laminar flame speeds of methane for the 35-step mechanism are the same as those of the 27-step mechanism, which are higher than experimental values. The 35-step mechanism can reproduce the laminar flame speed of n-heptane at an equivalence ratio of less than 0.9, however, the 27-step mechanism fails to predict the laminar flame speeds of n-heptane at all equivalence ratios.

However, for practical application like engine combustion simulation, these two newly developed mechanisms give reasonabe predictions of ignition timings, in-cylinder pressures, HRRs, CA10, power output, ISFC, and soot emissions in a HPDI natural gas marine engine model. During the engine design process, efficient and robust CFD simulation is the key factor. In comparison to the 334-step mechanism, the 27- and 35-step mechanism are sufficient in the predictions of both the overall engine combustion performance and detailed in-cylinder combustion processes. As a consequence, for the complex combustion process in engines, whether a precise kinetic model is necessary for the research and development of ICEs remains to be further explored. After all, the complex mechanism makes it very difficult for engine simulations. Of course, the 27- and 35-step reduced mechanisms also require to be further validated extensively at other engine operating conditions

4. Conclusions

In the present study, two reduced n-heptane/methane mechanisms were constructed by employing various reduction

approaches, including the reaction pathway analysis, sensitivity analysis, and the HyChem method. In addition, the reaction rate constants were optimized based on the sensitivity analysis of ignition delays. The reduced mechanisms were validated against the experimental ignition delays, laminar flame speeds, and engine combustion and emission results.

The 27- and 35-step mechanisms can well predict the experimental ignition delays of the n-heptane/air and methane/air mixtures. The calculated laminar flame speeds of the n-heptane/air and methane/air mixtures for these two reduced mechanisms are only in agreement with the experimental data at the stoichiometric and lean mixture conditions.

The applications of the 27- and 35-step reduced mechanisms in the multi-dimensional CFD simulations can significantly shorten the CPU-hours. Both the 27- and 35-step mechanisms could reasonably predict the experimental engine combustion process and NOx emissions. And the distributions of temperature, equivalence ratio, OH, CH_2O, NOx, and soot calculated by the 35- and 27-step mechanisms are in reasonable agreement with those calculated by the 334-step mechanism at 0° CA ATDC. As a result, the present reduced n-heptane/methane mechanisms can be used for the future design of the HPDI natural gas marine engines.

In the future, owing to the complicated combustion process in engines, whether a precise kinetic model is necessary for the engine research and design needs to be further explored. After all, the more complicated mechanism makes it more expensive and time-consuming for engine simulations. Of course, the 27- and 35-step reduced mechanisms also require to be further validated at more engine-related conditions.

Acknowledgement

This work was supported by the National Natural Science Foundation of China (NSFC) through its project of 91941102 and 51922076.

References

[1] Wei H, Qi J, Zhou L, Zhao W, Shu G. Ignition Characteristics of Methane/n-Heptane Fuel Blends under Engine-like Conditions. Energy & Fuels 2018;32(5):6264-77.

[2] He Y, Wang Y, Grégoire C, Niedzielska U, Mével R, Shepherd JE. Ignition characteristics of dual-fuel methane-n-hexane-oxygen-diluent mixtures in a rapid compression machine and a shock tube. Fuel 2019;249:379-91.

[3] McTaggart-Cowan G, Huang J, Munshi S. Impacts and Mitigation of Varying Fuel Composition in a Natural Gas

Heavy-Duty Engine. SAE International Journal of Engines 2017;10(4):1506-17.

[4] McTaggart-Cowan GP, Jones HL, Rogak SN, Bushe WK, Hill PG, Munshi SR. The Effects of High-Pressure Injection on a Compression–Ignition, Direct Injection of Natural Gas Engine. Journal of Engineering for Gas Turbines and Power 2006;129(2):579-88.

[5] Wagemakers AMLM, Leermakers CAJ. Review on the Effects of Dual-Fuel Operation, Using Diesel and Gaseous Fuels, on Emissions and Performance. *SAE Technical Paper Series.* 2012.

[6] Zeng K, Huang Z, Liu B, Liu L, Jiang D, Ren Y, et al. Combustion characteristics of a direct-injection natural gas engine under various fuel injection timings. Appl Therm Eng 2006;26(8-9):806-13.

[7] Liu H, Li J, Wang J, Wu C, Liu B, Dong J, et al. Effects of injection strategies on low‐speed marine engines using the dual fuel of high‐pressure direct‐injection natural gas and diesel. Energy Science & Engineering 2019.

[8] Cho HM, He B-Q. Spark ignition natural gas engines—A review. Energy Convers Manage 2007;48(2):608-18.

[9] Roethlisberger RP, Favrat D. Investigation of the prechamber geometrical configuration of a natural gas spark ignition engine for cogeneration: part I. Numerical simulation. International Journal of Thermal Sciences 2003;42(3):223-37.

[10] Florea R, Neely GD, Abidin Z, Miwa J. Efficiency and Emissions Characteristics of Partially Premixed Dual-Fuel Combustion by Co-Direct Injection of NG and Diesel Fuel (DI2). *SAE Technical Paper Series.* 2016.

[11] Huang Z, Shiga S, Ueda T, Nakamura H, Ishima T, Obokata T, et al. Effect of Fuel Injection Timing Relative to Ignition Timing on the Natural-Gas Direct-Injection Combustion. Journal of Engineering for Gas Turbines and Power 2002;125(3):783-90.

[12] Demosthenous E, Borghesi G, Mastorakos E, Cant RS. Direct Numerical Simulations of premixed methane flame initiation by pilot n-heptane spray autoignition. Combust Flame 2016;163:122-37.

[13] Demosthenous E, Mastorakos E, Stewart Cant R. Direct Numerical Simulations of Dual-Fuel Non-Premixed Autoignition. Combust Sci Technol 2016;188(4-5):542-55.

[14] Curran HJ, Gaffuri P, Pitz WJ, Westbrook CK. A comprehensive modeling study of n-heptane oxidation. Combust Flame 1998;114(1-2):149-77.

[15] Zhang K, Banyon C, Bugler J, Curran HJ, Rodriguez A, Herbinet O, et al. An updated experimental and kinetic modeling study of n- heptane oxidation. Combust Flame 2016;172:116-35.

[16] Ciezki HK, Adomeit G. Shock-tube investigation of self-ignition of n-heptane-air mixtures under engine relevant conditions. Combust Flame 1993;93(4):421-33.

[17] Davidson DF, Hanson RK. Interpreting shock tube ignition data. Int J Chem Kinet 2004;36(9):510-23.

[18] Fieweger K, Blumenthal R, Adomeit G. Self-ignition of S.I. engine model fuels: A shock tube investigation at high pressure. Combust Flame 1997;109(4):599-619.

[19] Gauthier BM, Davidson DF, Hanson RK. Shock tube determination of ignition delay times in full-blend and surrogate fuel mixtures. Combustion and Flame 2004;139(4):300-11.

[20] Hu E, Li X, Meng X, Chen Y, Cheng Y, Xie Y, et al. Laminar flame speeds and ignition delay times of methane–air mixtures at elevated temperatures and pressures. Fuel 2015;158:1-10.

[21] Huang J, Hill PG, Bushe WK, Munshi SR. Shock-tube study of methane ignition under engine-relevant conditions: experiments and modeling. Combust Flame 2004;136(1-2):25-42.

[22] Liang J, Zhang Z, Li G, Wan Q, Xu L, Fan S. Experimental and kinetic studies of ignition processes of the methane–n-heptane mixtures. Fuel 2019;235:522-9.

[23] Davis SG, Law CK, Wang H. Propene pyrolysis and oxidation kinetics in a flow reactor and laminar flames. Combust Flame 1999;119(4):375-99.

[24] Held TJ, Marchese AJ, Dryer FL. A Semi-Empirical Reaction Mechanism for n-Heptane Oxidation and Pyrolysis. Combust Sci Technol 1997;123(1-6):107-46.

[25] Zhang Z, Zhao H, Cao L, Li G, Ju Y. Kinetic Effects of n-Heptane Addition on Low and High Temperature Oxidation

of Methane in a Jet-Stirred Reactor. Energy & Fuels 2018;32(11):11970-8.

[26] Griffiths JF, Halford-Maw PA, Rose DJ. Fundamental features of hydrocarbon autoignition in a rapid compression machine. Combust Flame 1993;95(3):291-306.

[27] Minetti R, Carlier M, Ribaucour M, Therssen E, Sochet LR. A rapid compression machine investigation of oxidation and auto-ignition of n-Heptane: Measurements and modeling. Combust Flame 1995;102(3):298-309.

[28] Tanaka S, Ayala F, Keck JC. A reduced chemical kinetic model for HCCI combustion of primary reference fuels in a rapid compression machine. Combust Flame 2003;133(4):467-81.

[29] Grogan KP, Scott Goldsborough S, Ihme M. Ignition regimes in rapid compression machines. Combust Flame 2015;162(8):3071-80.

[30] Aroonsrisopon T, Sohm V, Werner P, Foster DE, Morikawa T, Iida M. An Investigation Into the Effect of Fuel Composition on HCCI Combustion Characteristics. *SAE Technical Paper Series.* 2002.

[31] Aroonsrisopon T, Werner P, Waldman JO, Sohm V, Foster DE, Morikawa T, et al. Expanding the HCCI Operation With the Charge Stratification. *SAE Technical Paper Series.* 2004.

[32] Andrae J, Johansson D, Björnbom P, Risberg P, Kalghatgi G. Co-oxidation in the auto-ignition of primary reference fuels and n-heptane/toluene blends. Combust Flame 2005;140(4):267-86.

[33] Seshadri K. Numerical and asymptotic studies of the structure of stoichiometric and lean premixed heptane flames. Combust Flame 1997;108(4):518-36.

[34] Peters N, Paczko G, Seiser R, Seshadri K. Temperature cross-over and non-thermal runaway at two-stage ignition of N-heptane. Combust Flame 2002;128(1-2):38-59.

[35] Li H, Miller DL, Cernansky NP. Development of a Reduced Chemical Kinetic Model for Prediction of Preignition Reactivity and Autoignition of Primary Reference Fuels. *SAE Technical Paper Series.* SAE International; 1996.

[36] Su W, Huang H. Development and calibration of a reduced chemical kinetic model of n-heptane for HCCI engine combustion. Fuel 2005;84(9):1029-40.

[37] Patel A, Kong S-C, Reitz RD. Development and Validation of a Reduced Reaction Mechanism for HCCI Engine Simulations. *SAE Technical Paper Series.* 2004.

[38] Maroteaux F, Noel L. Development of a reduced n-heptane oxidation mechanism for HCCI combustion modeling. Combust Flame 2006;146(1-2):246-67.

[39] Lapointe S, Zhang K, McNenly MJ. Reduced chemical model for low and high-temperature oxidation of fuel blends relevant to internal combustion engines. Proceedings of the Combustion Institute 2019;37(1):789-96.

[40] Gustavsson J, Golovitchev VI. Spray Combustion Simulation Based on Detailed Chemistry Approach for Diesel Fuel Surrogate Model. *SAE Technical Paper Series.* SAE International; 2003.

[41] Zheng J, Yang W, Miller DL, Cernansky NP. A Skeletal Chemical Kinetic Model for the HCCI Combustion Process. *SAE Technical Paper Series.* SAE International; 2002.

[42] Ra Y, Reitz RD. A reduced chemical kinetic model for IC engine combustion simulations with primary reference fuels. Combustion and Flame 2008;155(4):713-38.

[43] Heufer KA, Olivier H. Determination of ignition delay times of different hydrocarbons in a new high pressure shock tube. Shock Waves 2010;20(4):307-16.

[44] Wang H, Xu R, Wang K, Bowman CT, Hanson RK, Davidson DF, et al. A physics-based approach to modeling real-fuel combustion chemistry - I. Evidence from experiments, and thermodynamic, chemical kinetic and statistical considerations. Combust Flame 2018;193:502-19.

[45] Fieweger K, Blumenthal R, Adomeit G. Shock-tube investigations on the self-ignition of hydrocarbon-air mixtures at high pressures. Symposium (International) on Combustion 1994;25(1):1579-85.

[46] Kumar K, Freeh JE, Sung CJ, Huang Y. Laminar Flame Speeds of Preheated iso-Octane/O2/N2 and n-Heptane/O2/N2 Mixtures. Journal of Propulsion and Power 2007;23(2):428-36.

[47] Smallbone AJ, Liu W, Law CK, You XQ, Wang H. Experimental and modeling study of laminar flame speed and

non-premixed counterflow ignition of n-heptane. Proceedings of the Combustion Institute 2009;32(1):1245-52.

[48] Ji C, Dames E, Wang YL, Wang H, Egolfopoulos FN. Propagation and extinction of premixed C5–C12 n-alkane flames. Combustion and Flame 2010;157(2):277-87.

[49] Kelley AP, Smallbone AJ, Zhu DL, Law CK. Laminar flame speeds of C5 to C8 n-alkanes at elevated pressures: Experimental determination, fuel similarity, and stretch sensitivity. Proceedings of the Combustion Institute 2011;33(1):963-70.

[50] Dirrenberger P, Glaude PA, Bounaceur R, Le Gall H, da Cruz AP, Konnov AA, et al. Laminar burning velocity of gasolines with addition of ethanol. Fuel 2014;115:162-9.

[51] Li G, Liang J, Zhang Z, Tian L, Cai Y, Tian L. Experimental Investigation on Laminar Burning Velocities and Markstein Lengths of Premixed Methane–n-Heptane–Air Mixtures. Energy & Fuels 2015;29(7):4549-56.

[52] Bradley D. Burning velocities, markstein lengths, and flame quenching for spherical methane-air flames: A computational study. Combustion and Flame 1996;104(1-2):176-98.

[53] Hassan M. Measured and predicted properties of laminar premixed methane/air flames at various pressures. Combustion and Flame 1998;115(4):539-50.

[54] Vagelopoulos CM, Egolfopoulos FN. Direct experimental determination of laminar flame speeds. Symposium (International) on Combustion 1998;27(1):513-9.

[55] Dyakov IV, Konnov AA, Ruyck JD, Bosschaart KJ, Brock ECM, De Goey LPH. Measurement of Adiabatic Burning Velocity in Methane-Oxygen-Nitrogen Mixtures. Combustion Science and Technology 2001;172(1):81-96.

[56] Tahtouh T, Halter F, Mounaïm-Rousselle C. Measurement of laminar burning speeds and Markstein lengths using a novel methodology. Combustion and Flame 2009;156(9):1735-43.

[57] Dirrenberger P, Le Gall H, Bounaceur R, Herbinet O, Glaude P-A, Konnov A, et al. Measurements of Laminar Flame Velocity for Components of Natural Gas. Energy & Fuels 2011;25(9):3875-84.

[58] Richards KJ, Senecal PK, Pomraning E. CONVERGE Manual (Version 2.3). Madison, WI-USA: Convergent Science Inc.; 2016.

[59] Lavoie GA, Heywood JB, Keck JC. Experimental and Theoretical Study of Nitric Oxide Formation in Internal Combustion Engines. Combustion Science and Technology 1970;1(4):313-26.

[60] Hiroyasu H, Kadota T, Arai M. Development and Use of a Spray Combustion Modeling to Predict Diesel Engine Efficiency and Pollutant Emissions : Part 1 Combustion Modeling. Bulletin of JSME 1983;26(214):569-75.

[61] Li J, Wang J, Liu T, Dong J, Liu B, Wu C, et al. An Investigation of the Influence of Gas Injection Rate Shape on High-Pressure Direct-Injection Natural Gas Marine Engines. Energies 2019;12(13).

[62] LARSON CR. Injection Study of a Diesel Engine Fueled With Pilot ‐ Ignited, Directly ‐ Injected Natural gas. Canada: University of British Columbia; 2003.

[63] Jud M, Fink G, Sattelmayer T. Predicting Ignition and Combustion of a Pilot Ignited Natural Gas Jet Using Numerical Simulation Based on Detailed Chemistry. *Volume 2: Emissions Control Systems; Instrumentation, Controls, and Hybrids; Numerical Simulation; Engine Design and Mechanical Development.* 2017.